ELSEVIER

Journal of Organometallic Chemistry 573 (1999) 171–179

Journal of Organometallic Chemistry

Syntheses, structures and magnetism of homoleptic complexes of 4-{pyrid-4-yloxy}-2,2,6,6-tetramethyl-1-piperidinoxyl, a new spin-labelled pyridine[1]

Malcolm A. Halcrow [a,*], Lide M. Rodriguez-Martinez [a,b], Euan K. Brechin [c], John E. Davies [a], Ian J. Scowen [d,e], Mary McPartlin [d]

[a] *Department of Chemistry, University of Cambridge, Lensfield Road, Cambridge CB2 1EW, UK*
[b] *Interdisciplinary Research Centre in Superconductivity, University of Cambridge, Madingley Road, Cambridge CB3 0HE, UK*
[c] *Department of Chemistry, The University of Edinburgh, West Mains Road, Edinburgh EH9 3JJ, UK*
[d] *School of Applied Chemistry, University of North London, 166-220 Holloway Road, London N7 8DB, UK*
[e] *Department of Chemistry and Chemical Technology, University of Bradford, Bradford BD7 1DP, UK*

Received 27 March 1998

Abstract

Reaction of 4-chloropyridine hydrochloride with 4-hydroxy-2,2,6,6-tetramethyl-1-piperidinoxyl in the presence of five equivalents of powdered KOH in DMSO at 30°C affords L^1 in 10–50% yield after an aqueous quench. The complexes $[M(L^1)_4](BF_4)_2$ (M = Ni, **1**; M = Cu, **2**; M = Pd, **3**) have been prepared by complexation of hydrated $M(BF_4)_2$ (M = Ni, Cu), or $[PdCl_2(NCPh)_2] + 2AgBF_4$, by four equivalents of L^1 in MeCN. Diffusion of Et_2O into MeCN solutions of **2** affords two crystalline polymorphs of this complex, both containing square planar $[Cu(L^1)_4]^{2+}$ dications [Cu–N = 2.005(7)–2.042(6) Å]. The major, monoclinic form contains axial Cu…NCMe contacts of 2.394(7) and 2.859(8) Å, while the minor, triclinic form exhibits long axial Cu…FBF_3 bonds (Cu…F = 2.478(5), 2.551(5) Å). In both structures, the Cu…N(nitroxyl) distances are 9.5–9.7 Å. The *Q*-band EPR spectrum of **2** in 10:1 MeCN:toluene solution at 293 K is a broad featureless line, suggesting $|J_{Cu\text{-}L}1| \geq 0.07\ cm^{-1}$. Variable temperature susceptibility measurements on powdered **2** and **3** show weakly antiferromagnetic behaviour. For **2** these data are well reproduced both by the Curie–Weiss law and by a model describing intramolecular superexchange; for **3**, the data could not be fit satisfactorily, suggesting the presence of a significant intermolecular superexchange pathway.

Keywords: Spin-label; Nickel; Copper; Palladium; Crystal structure; Superexchange

1. Introduction.

The magnetic properties of complexes of spin-labelled ligands continue to be widely studied. In addition to fundamental interest aimed at elucidating in detail the structural factors mediating the sign and magnitude of superexchange between a metal complex and a pendant organic radical [1,2], spin labelled ligands and their complexes have been used as structural probes of metalloenzyme active sites [1,2], metal/DNA interactions [3,4], and of micellar [5] and dendrimeric [6] macrostructures. We report here the facile synthesis of a new TEMPO-substituted pyridine (TEMPO = 2,2,6,6-tetramethyl-1-piperidinoxyl), together with a study of its complex chemistry.

* Corresponding author. E-mail: Malcolm.Halcrow@ch.cam.ac.uk
[1] Dedicated to Brian Johnson on the occasion of his 60th birthday.

0022-328X/99/$ - see front matter
PII S0022-328X(98)00654-8

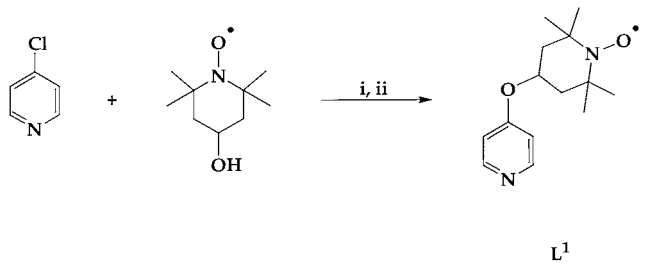

L^1

Scheme 1. (i) Five equivalents KOH, DMSO, 30°C, 6 h; (ii) H_2O, room temperature.

2. Experimental

2.1. Reagents

All manipulations were performed in air using commercial grade solvents. 4-Chloropyridine hydrochloride, 4-hydroxy-TEMPO, $Ni(BF_4)_2 \cdot 6H_2O$, $Cu(BF_4)_2 \cdot xH_2O$ (x ca. 4; Aldrich), $AgBF_4$ (Avocado) were used as supplied. $[PdCl_2(NCPh)_2]$ was prepared by the literature procedure [7].

2.2. Syntheses

2.2.1. Synthesis of 4-(pyridin-4-yloxy)-2,2,6,6-tetramethyl-1-piperidinoxyl (L^1)

To a suspension of freshly ground KOH (3.30 g, 5.90×10^{-2} mol) in DMSO (35 cm^3) was added 4-hydroxy-TEMPO (2.00 g, 1.18×10^{-2} mol) and 4-chloropyridine hydrochloride (1.77 g, 1.18×10^{-2} mol) in that order. The mixture was stirred at 30°C for 6 h, then quenched with an equal volume of water and allowed to stand at room temperature. Rose-coloured platelets of L^1 precipitated over the course of 3 h, which were filtered, washed with water until the washings were neutral, and dried over P_2O_5. The product was analysed without further purification (1.4 g, 48%). (Found: C, 67.1; H, 8.5; N, 11.1. $C_{14}H_{21}N_2O_2$ requires C, 67.4; H, 8.5; N, 11.2%). M.p. 111–113°C. FAB mass spectrum: m/z 251 $[M+2H]^+$, 250 $[M+H]^+$, 249 $[M]^+$, 235 $[M-CH_3+H]^+$. UV/vis (MeCN) λ_{max}, nm (ε_{max}, M^{-1} cm^{-1}) 219 (10600), 240 (sh), 450 (12). ^1H NMR (CD_3CN, 293K): δ, ppm 9.2 (TEMPO equatorial CH_3), 8.4 (Py $H^{2/6}$), 7.1 (Py $H^{3/5}$), −2.6 (TEMPO H^4).

2.2.2. Synthesis of tetrakis-[4-(pyridin-4-yloxy)-2,2,6,6-tetramethyl-1-piperidinoxyl]nickel(II) ditetrafluoroborate (**1**)

A mixture of L^1 (0.20 g, 8.03×10^{-4} mol) and $Ni(BF_4)_2 \cdot 6H_2O$ (0.062 g, 2.01×10^{-4} mol) was stirred in MeCN (20 cm^3) at room temperature for 15 min. The resultant red solution was reduced to ca. 3 cm^3 volume and filtered. Vapour diffusion of Et_2O into this solution afforded orange microcrystals, which were dried in vacuo. Yield 0.20 g, 82%. (Found: C, 53.1; H, 6.9; N, 9.1%. $C_{56}H_{84}B_2F_8N_8NiO_8 \cdot H_2O$ requires C, 53.9; H, 7.0; N, 9.0%). FAB mass spectrum: m/z 557 $[^{58}Ni(L^1)_2+H]^+$, 541 $[^{58}Ni(L^1)_2-CH_3]^+$, 526

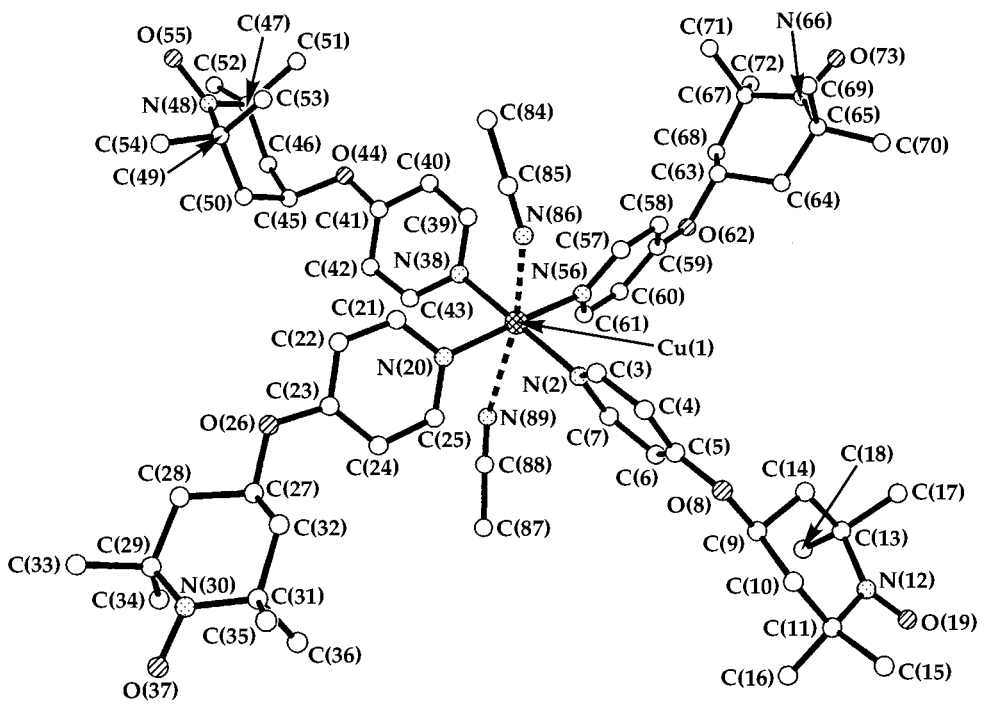

Fig. 1. Solid state structure of the $[Cu(L^1)_4(NCMe)_2]^{2+}$ dication in α-**2**·3MeCN, showing the atom numbering scheme employed. For clarity, all hydrogen atoms have been omitted.

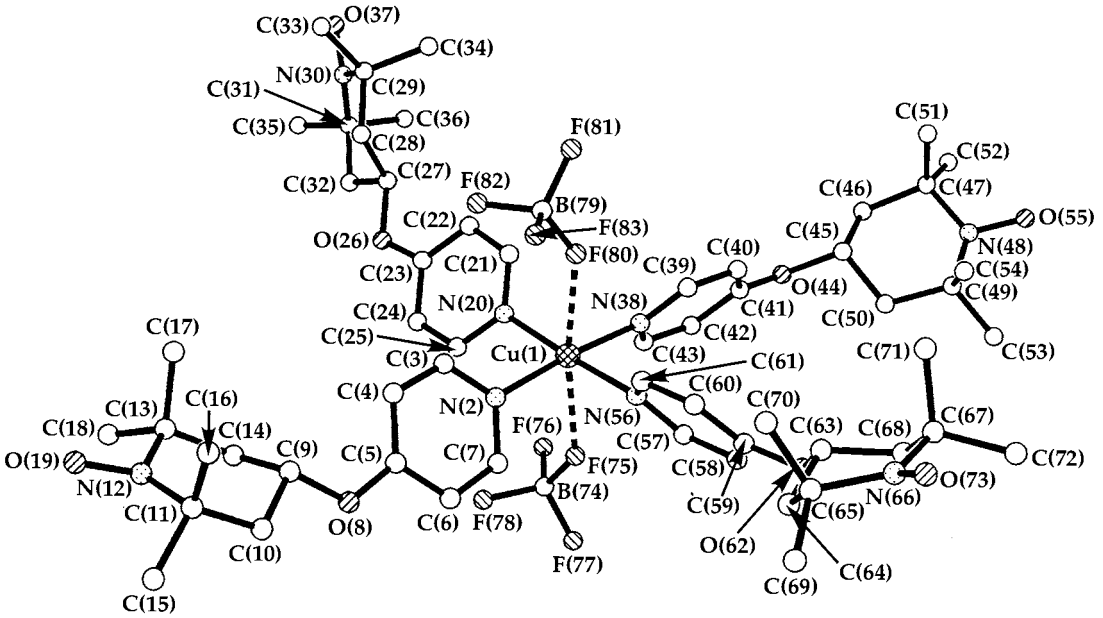

Fig. 2. Solid state structure of the $[Cu(L^1)_4(BF_4)_2]$ molecule in β-**2**·3MeCN·0.5H_2O, showing the atom numbering scheme employed. For clarity, all hydrogen atoms have been omitted.

$[^{58}Ni(L^1)_2-2CH_3]^+$, 402 $[^{58}Ni(L^1)(L^1-TEMPO)]^+$, 251 $[L^1+2H]^+$, 250 $[L^1+H]^+$, 249 $[L^1]^+$. UV/vis (MeCN): λ_{max}, nm (ε_{max}, $M^{-1}.cm^{-1}$) 219 (48,200), 235 (sh), 245 (sh), 361 (18), 464 (41), 927 (6.3). UV/vis ($MeNO_2$): λ_{max}, nm (ε_{max}, $M^{-1}\,cm^{-1}$), 453 (46), 593 (sh), 962 (6.3). UV/vis (KBr disk): λ_{max}, nm 455. ^1H NMR (CD_3CN, 293K): δ, ppm 41.2 (Py $H^{3/5}$), 10.3 (TEMPO equatorial CH_3), −0.5 (TEMPO H^4).

2.2.3. Synthesis of tetrakis-[4-(pyridin-4-yloxy)-2,2,6,6-tetramethyl-1-piperidinoxyl]copper(II) ditetrafluoroborate (**2**)

Method as for **1**, employing $Cu(BF_4)_2\cdot xH_2O$ (0.062 g, 2.01×10^{-4} mol). The product formed large mauve blocks from $MeCN/Et_2O$ (0.21 g, 85%). (Found: C, 53.4; H, 6.8; N, 8.8%. $C_{56}H_{84}B_2CuF_8N_8O_8\cdot H_2O$ requires C, 53.7; H, 6.9; N, 9.0%). FAB mass spectrum: m/z 562 $[^{63}Cu(L^1)_2+H]^+$, 546 $[^{63}Cu(L^1)_2-CH_3]^+$, 531 $[^{63}Cu(L^1)_2-2CH_3]^+$, 407 $[^{63}Cu(L^1)(L^1-TEMPO)]^+$, 251 $[L^1+2H]^+$, 250 $[L^1+H]^+$, 249 $[L^1]^+$. UV/vis (MeCN): λ_{max}, nm (ε_{max}, $M^{-1}\,cm^{-1}$) 215 (58800), 236 (sh), 453 (sh), 573 (78). UV/vis ($MeNO_2$): λ_{max}, nm (ε_{max}, $M^{-1}\,cm^{-1}$) 459 (sh), 557 (72). UV/vis (KBr disk): λ_{max}, nm 578.

2.2.4. Synthesis of tetrakis-[4-(pyridin-4-yloxy)-2,2,6,6-tetramethyl-1-piperidinoxyl]palladium(II) ditetrafluoroborate (**3**)

A mixture of L^1 (0.20 g, 8.03×10^{-4} mol), $[PdCl_2(NCPh)_2]$ (0.077 g, 2.01×10^{-4} mol) and $AgBF_4$ (0.079 g, 4.02×10^{-4} mol) was stirred in MeCN (20 cm^3) at room temperature for 2 h. The AgCl precipitate was removed by filtration, and the orange solution was reduced to ca. 3 cm^3 volume. Vapour diffusion of Et_2O into this solution afforded a bright orange polycrystalline solid, which was dried in vacuo (0.21 g, 82%). (Found: C, 52.6; H, 6.7; N, 9.2%. $C_{56}H_{84}B_2F_8N_8O_8Pd$ requires C, 52.7; H, 6.6; N, 8.8%). FAB mass spectrum: m/z 853 $[^{106}Pd(L^1)_3]^+$, 838 $[^{106}Pd(L^1)_3-CH_3]^+$, 604 $[^{106}Pd(L^1)_2]^+$, 589 $[^{106}Pd(L^1)_2-CH_3]^+$, 574 $[^{106}Pd(L^1)_2-2CH_3]^+$, 450 $[^{106}Pd(L^1)(L^1-TEMPO)]^+$, 355 $[^{106}Pd(L^1)]^+$, 250 $[L^1+H]^+$, 249 $[L^1]^+$. UV/vis (MeCN): λ_{max}, nm (ε_{max}, $M^{-1}\,cm^{-1}$) 240 (85800), 270 (sh), 278 (16900), 320 (10300), 330 (sh), 459 (42). ^1H NMR spectrum (CD_3CN, 293K): δ, ppm 8.5 (Py $H^{2/6}$), 7.8 (Py $H^{3/5}$), −1.0 (TEMPO H^4).

2.3. Single crystal X-ray structure determinations

Vapour diffusion of Et_2O into dilute solutions of **2** MeCN afforded large mauve blocks of this complex. Although the sample of **2** was visually homogeneous, examination of several crystals demonstrated the presence of major and minor polymorphs of monoclinic and triclinic symmetry, respectively. Experimental details for the structure determinations are given in Table 2. Both structures were solved by direct methods (SHELXTL Plus [8]) and refined by full matrix least-squares on F^2 (SHELXL 93 [9]), with H atoms placed in calculated positions. Atomic coordinates, bond lengths and angles and thermal parameters for both structures have been deposited at the Cambridge Crystallographic Data Centre.

2.3.1. X-ray structure determination of $[Cu(L^1)_4](BF_4)_2 \cdot 3CH_3CN$ (α-**2**·3MeCN)

In addition to the two molecules of MeCN associated with Cu(1), 1 additional molecule of lattice MeCN was also present in the unit cell. No disorder in this structure was detected during refinement. All non-H atoms were refined anisotropically, and no restraints were applied.

2.3.2. X-ray structure determination of $[Cu(L^1)_4](BF_4)_2 \cdot 3CH_3CN \cdot 0.5H_2O$ (β-**2**·3MeCN·0.5H_2O)

Two datasets on this polymorph were collected, both of which diffracted poorly at high angle. Four molecules of lattice acetonitrile were detected during refinement. Two of these [C(84)–N(86) and C(87)–N(89)] were modelled as wholly occupied, while two others [C(90)–N(92) and C(93)–N(95)], which lie within a highly disordered region of electron density, were given occupancies of 0.5. The C–C and C≡N bond lengths within these solvent molecules were restrained to common values, which refined to 1.39(2) and 1.14(2) Å respectively. Finally, a weakly scattering feature that was not bonded to any other molecule in the asymmetric unit was modelled as half a molecule of water. The two largest peaks of residual electron density lie within the aforementioned region of disordered solvent. All non-H atoms within the complex cation and BF_4^- anions, which were not disordered, were refined anisotropically, while the lattice solvent atoms were refined isotropically.

Table 1
Selected bond lengths (Å) and bond angles (°) for the structures of α-$[Cu(L^1)_4](BF_4)_2 \cdot 3MeCN$ and β-$[Cu(L^1)_4](BF_4)_2 \cdot 3MeCN \cdot 0.5H_2O$[a]

	α-Form	β-Form
Cu(1)–N(2)	2.009(5)	2.020(6)
Cu(1)–N(20)	2.022(5)	2.005(7)
Cu(1)–N(38)	2.026(5)	2.042(6)
Cu(1)–N(56)	2.013(6)	2.012(7)
Cu(1)–X(1)	2.394(7)	2.551(5)
Cu(1)–X(2)	2.859(8)	2.478(5)
N(12)–O(19)	1.275(7)	1.287(8)
N(30)–O(37)	1.293(7)	1.299(8)
N(48)–O(55)	1.304(8)	1.274(9)
N(66)–O(73)	1.271(7)	1.293(9)
N(2)–Cu(1)–N(20)	92.8(2)	92.0(3)
N(2)–Cu(1)–N(38)	173.8(3)	174.8(3)
N(2)–Cu(1)–N(56)	88.9(2)	89.6(3)
N(2)–Cu(1)–X(1)	97.2(2)	89.2(2)
N(2)–Cu(1)–X(2)	89.6(2)	96.3(2)
N(20)–Cu(1)–N(38)	90.9(2)	90.2(3)
N(20)–Cu(1)–N(56)	174.4(3)	177.2(3)
N(20)–Cu(1)–N(X1)	90.0(2)	96.0(2)
N(20)–Cu(1)–N(X2)	82.8(2)	88.7(2)
N(38)–Cu(1)–N(56)	87.0(2)	88.4(3)
N(38)–Cu(1)–N(X1)	87.8(2)	85.8(2)
N(38)–Cu(1)–N(X2)	86.0(2)	88.5(2)
N(56)–Cu(1)–N(X1)	95.1(2)	86.4(2)
N(56)–Cu(1)–N(X2)	91.9(2)	88.8(2)
X(1)–Cu(1)–N(X2)	170.4(2)	172.6(2)

[a] α-form; X(1) = N(86), X(2) = N(89): β-form; X(1) = F(75), X(2) = F(80).

Table 2
Experimental details for the single crystal structure determinations in this study

	α-**2**·3MeCN	β-**2**·3MeCN·0.5H_2O
Formula	$C_{62}H_{93}B_2CuF_8N_{11}O_8$	$C_{62}H_{94}B_2CuF_8N_{11}O_{8.5}$
M_r	1357.63	1366.64
Crystal habit	Mauve lath	Mauve block
Crystal size (mm)	0.50 × 0.40 × 0.20	0.50 × 0.40 × 0.40
Crystal class	Monoclinic	Triclinic
Space group	$P2_1$	$P\bar{1}$
a (Å)	15.181(4)	14.213(9)
b (Å)	15.044(6)	14.763(8)
c (Å)	15.220(5)	20.879(10)
α (°)	—	106.27(5)
β (°)	90.83(2)	93.30(6)
γ (°)	—	115.97(4)
U (Å^3)	3476(2)	3697(4)
Z	2	2
D_{calc} (mg m^{-3})	1.297	1.227
Radiation (λ, Å)	Mo–K_α (0.71069)	Mo–K_α (0.71069)
No. of reflections for lattice parameters	25	25
μ (mm^{-1})	0.394	0.372
F(000)	1434	1442
Temperature (K)	150(2)	150(2)
Diffractometer	Rigaku AFC7R	Rigaku AFC5R
Scan type	ω–2θ	ω–2θ
Absorption correction	Semi-empirical (Ψ-scans)	Semi-empirical (Ψ-scans)
Min. transmission	0.846	0.967
Max. transmission	1.000	1.000
Measured reflections	6580	12123
Independent reflections (R_{int})	6328 (0.0580)	11 614 (0.0723)
Observed reflections ($I > 2\sigma(I)$)	4870	6083
Range in θ (°)	$3 \le \theta \le 25$	$3 \le \theta \le 24$
Standards	3 every 200 reflections	3 every 200 reflections
Variation (%)	−2.0	−0.9
Range in h	$0 \le h \le 18$	$-16 \le h \le 14$
Range in k	$0 \le k \le 17$	$0 \le k \le 16$
Range in l	$-18 \le l \le 18$	$-23 \le l \le 22$
Refinement on	F^2	F^2
No. of parameters	848	822
No. of restraints	1	8
$R(F)$	0.0565	0.0942
$wR(F^2)$	0.1417	0.3149
Goodness-of-fit	1.039	1.011
Weighting scheme	$w = 1/[\sigma^2(F_o^2) + (0.0611P)^2 + 2.4598P]$	$w = 1/[\sigma^2(F_o^2) + (0.1587P)^2 + 6.9867P]$
Max. shift/estimated S.D.	0.033	0.012
$\Delta\rho_{min}$ (e Å^{-3})	−0.372	−1.024
$\Delta\rho_{max}$ (e Å^{-3})	0.474	1.282
Flack parameter	0.00(2)	

$R = \Sigma[|F_o| - |F_c|]/\Sigma|F_o|$, $wR = [\Sigma w(F_o^2 - F_c^2)/\Sigma wF_o^4]^{1/2}$, $P = (F_o^2 + 2F_c^2)/3$.

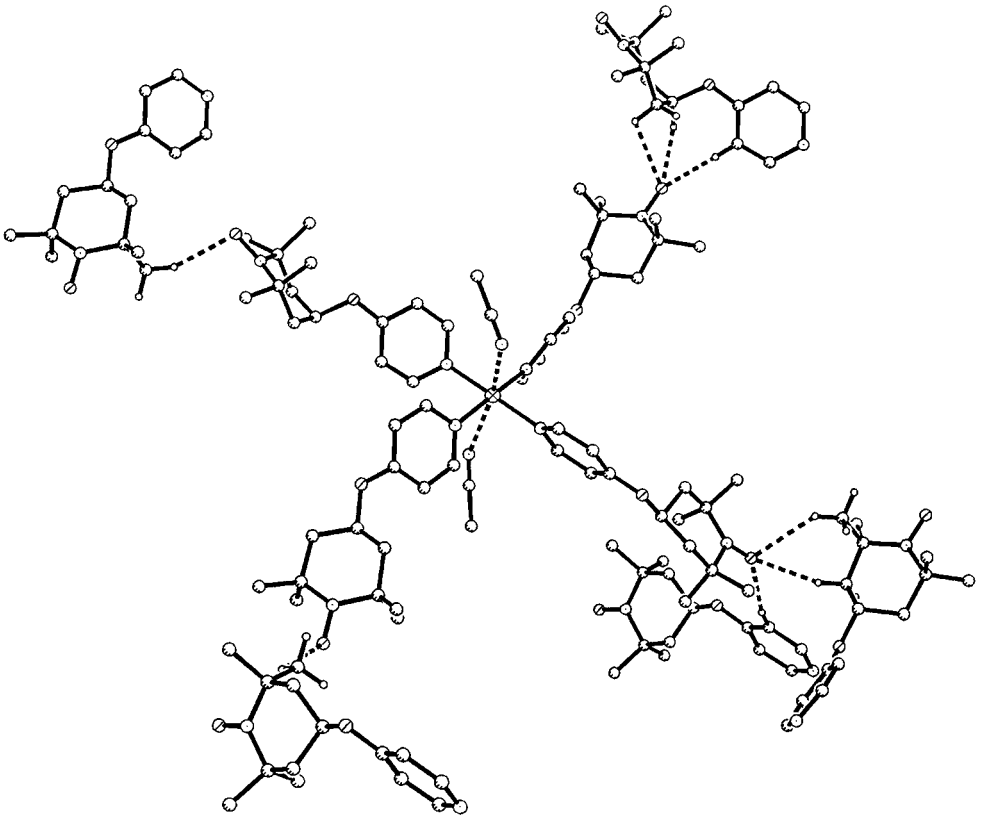

Fig. 3. Solid state structure of the $[Cu(L^1)_4(NCMe)_2]^{2+}$ dication in α-**2**·3MeCN, showing the intermolecular contacts involving the piperidinoxyl groups. For clarity, the BF_4^- anions and solvent molecules not taking part in these interactions are not shown, while only hydrogen atoms attached to carbon atoms involved in intermolecular N–O…H–C interactions are included.

2.4. Other measurements

Infrared spectra were obtained as Nujol mulls pressed between KBr windows between 400–4000 cm^{-1} using a Perkin-Elmer Paragon 1000 spectrophotometer. UV/visible spectra were obtained with a Perkin-Elmer Lambda 12 spectrophotometer operating between 200 and 1100 nm, in 1 cm quartz cells. All ^1H NMR spectra were run on a Bruker DPX250 spectrometer, operating at 250.1 MHz. Positive ion fast atom bombardment (FAB) mass spectra were performed on a Kratos MS890 spectrometer, employing a 3-NOBA matrix. CHN microanalyses were performed by the University of Cambridge Department of Chemistry microanalytical service. Melting points are uncorrected. EPR spectra were obtained using a Bruker ESP300E spectrometer; *X*-band spectra employed a ER4102ST resonator and ER4111VT cryostat, while for *Q*-band spectra a ER5106QT resonator and an ER4118VT cryostat were used. Variable temperature magnetic susceptibility measurements were obtained using a Quantum Design SQUID magnetometer. Diamagnetic corrections for the samples were estimated from Pascal's constants [10]; diamagnetic corrections for the sample holders were also applied. Observed and calculated data were refined using SIGMAPLOT [11].

3. Results and discussion.

3.1. Synthesis and characterisation of the ligand and complexes.

Following a previously employed route to 4′-2,2′:6′,2″-terpyridyl ethers [12,13], equimolar amounts of 4-hydroxy-TEMPO and 4-chloropyridine hydrochloride were reacted in DMSO in the presence of five equivalents of freshly ground KOH at 30°C (Scheme 1). The reaction was followed by TLC (THF eluent), which showed that the concentration of the desired product in the reaction mixture reached a maximum after ca. 6 h. Quenching of the mixture with an equal volume of water caused the slow precipitation of rose-coloured platelets of the desired product L^1 in analytical purity. In contrast to the good reliability of this method when applied to spin-labelled terpyridyl ethers [14], the yields of this synthesis are somewhat variable, from 10 and 50%; we ascribe this to the thermal instability of 4-chloropyridine, which undergoes self-quaternisation upon mild heating [15].

The spectroscopic properties of L^1 are typical of organic nitroxyl radicals [16]. The IR spectrum of this ligand as a Nujol mull exhibits an N–O stretching vibration at 1366 cm^{-1}, while UV/visible spectroscopy

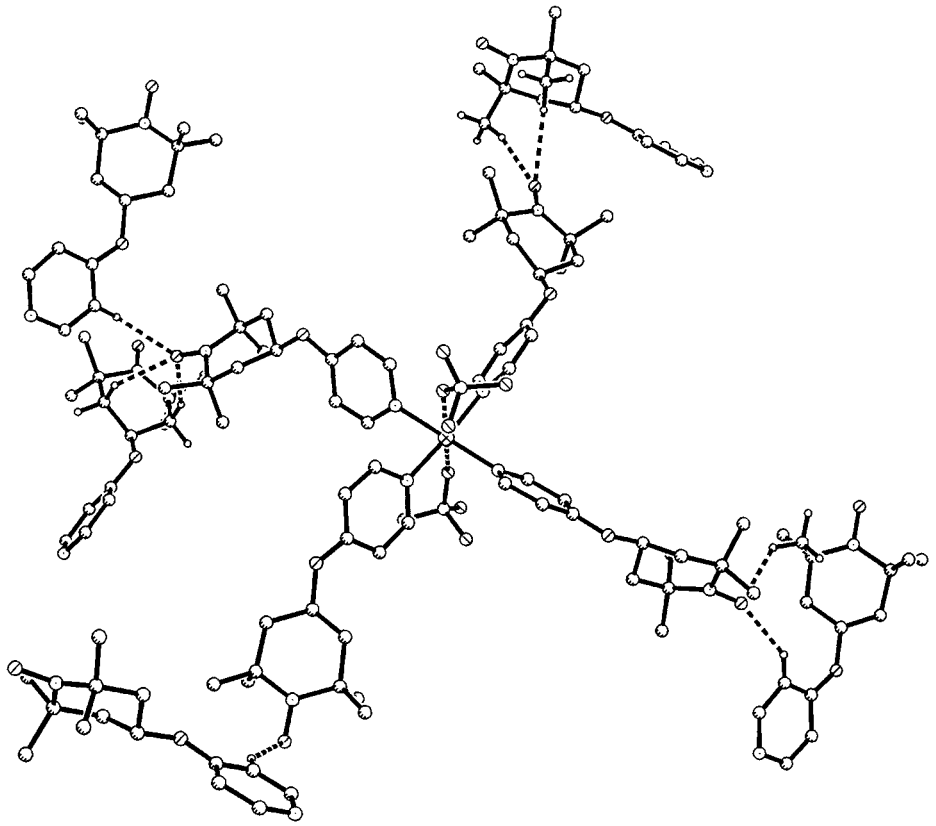

Fig. 4. Solid state structure of the $[Cu(L^1)_4(BF_4)_2]$ molecule in β-**2**·3MeCN·0.5H_2O, showing the intermolecular contacts involving the piperidinoxyl groups. For clarity, solvent molecules are not shown, while only hydrogen atoms attached to carbon atoms involved in intermolecular N–O…H–C interactions are included.

in MeCN shows, in addition to lower wavelength bands associated with the pyrid-4-yl substituent, a nitroxyl $n \rightarrow \pi^*$ absorption at $\lambda_{max} = 450$ nm ($\varepsilon_{max} = 12$ M^{-1} cm^{-1}). The *X*-band EPR spectrum of L^1 in mobile toluene solution is a three-line signal, with $< g > = 2.006$ and $< A\{^{14}N\} > = 13.6$ G. The ^1H NMR spectrum of L^1 in CD_3CN contains two paramagnetically broadened peaks of equal integral at δ 8.4 and 7.1 ppm, respectively ascribable to the $H^{2/6}$ and $H^{3/5}$ environments of the pyridyl ring. Two broader signals can also be discerned, centred at 9.2 and –2.6 p.p.m.; by comparison with the NMR spectrum of 4-hydroxy-TEMPO, which has been fully assigned [17], we tentatively assign these peaks respectively to the equatorial CH_3 and H^4 environments on the piperidinoxyl ring.

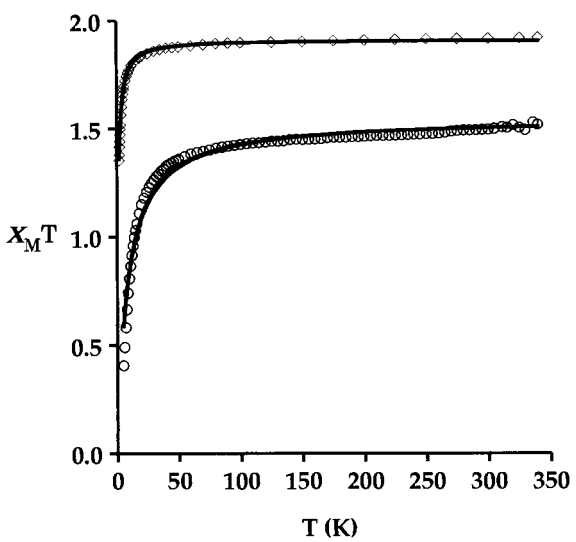

Fig. 5. Plots of X_MT versus T for solid **2** (◇) and **3** (○). The solid lines represent fits to the Curie–Weiss law; the fitting parameters are in the text.

Complexation of $Ni(BF_4)_2 \cdot 6H_2O$ by 4–6 molar equivalents of L^1 in MeCN in all cases yields a red solution, from which an orange microcrystalline solid can be obtained following vapour diffusion with Et_2O. Similar complexations employing $Cu(BF_4)_2 \cdot xH_2O$ (x ca. 4) give deep blue solutions, which yield large mauve blocks after an identical work-up. Both these solids desolvate in vacuo, the dried materials analysing as $[M(L^1)_4](BF_4)_2 \cdot H_2O$ (M = Ni, **1**; M = Cu, **2**). The IR spectra of **1** and **2** are consistent with the presence of L^1 and BF_4^- only. In particular, the ν(N–O) vibration in both these products is indistinguishable from that of free L^1, occurring at 1365 cm^{-1}. This suggests that L^1

is not coordinated through the nitroxyl O-atoms in these compounds. Complexes **1** and **2** were therefore formulated as containing 4 L^1 ligands coordinated through their pyridine N-donors, which precedent suggests should form a *trans*-axial six-coordinate geometry with weak axial ligation by anions and/or solvent [18]. This conclusion was confirmed by the crystallographic analysis of **2** described below.

The UV/vis spectra of **1** in MeCN or $MeNO_2$ solution exhibit *d–d* transitions at $\lambda_{max} = 930–960$ nm ($\varepsilon_{max} = 6\ M^{-1}\ cm^{-1}$) and 361 nm (18, MeCN only). These are consistent with 6-coordination at Ni [19], the third transition expected for this geometry probably being masked by the L^1 $n \rightarrow \pi^*$ absorption close to $\lambda_{max} = 455$ nm ($\varepsilon_{max} = 45\ M^{-1}\ cm^{-1}$). The ^1H NMR spectrum of **1** in CD_3CN confirms this conclusion, showing a peak at 41.2 ppm which is typical of a pyridyl $H^{3/5}$ environment at a paramagnetic Ni(II) centre [20]; there are no peaks attributable to **1** between 0–10 ppm in this spectrum. Presumably these data reflect the formation of *trans*-$[Ni(L^1)_4(solvent)_2]^{2+}$ species upon dissolution. As a KBr disk, **1** affords a very broad UV/vis absorption with a single maximum at $\lambda_{max} = 455$ nm, showing no discernable *d–d* transitions. The UV/vis spectrum of **2** in MeCN shows a *d–d* maximum at $\lambda_{max} = 573$ nm ($\varepsilon_{max} = 78\ M^{-1}\ cm^{-1}$), the nitroxyl $n \rightarrow \pi^*$ absorption occurring as a shoulder at 453 nm. This *d–d* band is observed at $\lambda_{max} = 557$ nm in $MeNO_2$, and at 578 nm as a KBr disk, these small differences suggesting that the solution and solid state structures of this compound are very similar.

In order to compare its magnetic properties with those of **2** (vide infra), we wished to prepare an analogous complex of L^1 using a diamagnetic metal centre. Given the uncertain spin state at Ni in solid **1**, the complex $[Pd(L^1)_4](BF_4)_2$ (**3**) was therefore prepared by reacting $[PdCl_2(NCPh)_2]$ [7] with four molar equivalents of L^1 in MeCN, using two equivalents of $AgBF_4$ as Cl^--abstractor. Complex **3** is isolated as an orange microcrystalline solid from $MeCN/Et_2O$, that rapidly desolvates in air. IR and UV/vis spectroscopic and microanalytical data for **3** were consistent with its formulation as the desired product, while the ^1H NMR spectrum of **3** in CD_3CN showed only small differences compared to uncomplexed L^1.

3.2. Single crystal X-ray structures

Vapour diffusion of Et_2O into moderately concentrated solutions of **2** in MeCN affords large deep blue blocks suitable for single crystal X-ray analysis. Examination of several crystals from two independent samples established the presence of two crystal forms of monoclinic (α) and triclinic (β) symmetries, with similar unit cell volumes. In each sample, the majority of the crystals examined were of the α-form. Presumably owing to substantial areas of disordered solvent within the asymmetric unit, crystals of the β-form diffracted relatively poorly. However, the molecule of interest in the β-form is well defined and free from disorder, so that some discussion of this structure is justified. Views of the complex molecules in the two forms are shown in Figs. 1 and 2, while selected metric parameters from the structures are listed in Table 1.

Both the α- and β-forms contain discrete $[Cu(L^1)_4]^{2+}$ cations, with Cu(1)–N bond lengths typical of Cu(II) *tetrakis*–pyridine complexes [21–23] and N–Cu(1)–N angles close to ideal values for square planarity (Fig. 1; Table 1). Both structures contain additional, weak axial ligation to the Cu ion. In the α-form, two MeCN molecules occupy the axial coordination sites, with Cu(1)–N(86) = 2.394(7) and Cu(1)–N(89) = 2.859(8) Å. This asymmetry in the axial Cu–N distances is reflected in a displacement of 0.09 Å of Cu(1) towards N(86) out of the least squares equatorial plane formed by N(2), N(20), N(38) and N(56). Both axial MeCN 'ligands' are substantially tilted from the line perpendicular to the N_4 equatorial plane, with Cu(1)–N(86)–C(85) = 149.7(6) and Cu(1)–N(89)–C(88) = 145.9(7)°. In the β-form, the axial coordination sites at Cu(1) are occupied by the two BF_4^- anions, with Cu(1)–F(75) = 2.551(5) and Cu(1)–F(80) = 2.478(5) Å. This structure thus resembles those previously reported for other $[Cu(py)_4]^{2+}$ complexes with weakly coordinating anions [21–23] although the only other crystallographically characterised tetrafluoroborate salt of this type, namely $[Cu(NC_5H_4NMe_2\text{-}4)_4](BF_4)_2$, exhibits longer axial Cu…F distances of 2.66 and 2.75 Å [21].

The N–O distances of the L^1 ligands in both structures lie in the range 1.271(7)–1.304(8) Å, which are typical values for nitroxyl radical centres [16]. All the piperidinoxyl rings in the complex molecules have the expected chair conformation, although in the α-form one ring [C(45)–O(55)] has the ether oxygen substituent O(44) in an axial, rather than an equatorial, position (Fig. 1). The average Cu…N(nitroxyl) distance in the α-form is 9.54 Å, while the intramolecular N…N distances between nitroxyl centres on adjacent ligands range from 12.505(9) to 14.368(9) Å; in the β-form, the corresponding values are 9.72 and 12.100(13)–14.519(14) Å.

The packing within the crystal lattice of **2** is of interest, since this can determine the sign of intermolecular magnetic interactions in solid nitroxyl compounds. In particular, close N–O…H–C contacts between one nitroxyl moiety and the methyl or methylene β-hydrogen atoms of a piperidinoxyl ring on a neighbouring molecule have been suggested to facilitate intermolecular ferromagnetism in TEMPO derivatives [24]. For both forms of **2**, there are eight intermolecular N–O…H–C contacts of < 2.8 Å, five of which are formed to the β-H atoms of neighbouring piperidinoxyl rings

(Figs. 3 and 4). It is therefore probable that the two polymorphs should exhibit similar magnetic behaviour.

3.3. EPR and magnetic studies.

Given that ligand dissociation from **2** in solution is low (vide supra), the EPR spectra of complexes of this type, containing $S = 1/2$ metal ions with spin-labelled ligands, can provide useful information regarding the strength of metal/nitroxyl superexchange [2]. The *X*- and *Q*-band EPR spectra of **2** in 10:1 MeCN:toluene at 293 K show, in addition to a weak triplet resonance from decoordinated L^1, a broad featureless line centred at $< g > = 2.02$. No half-field signal was detected in either of these spectra. In the strong exchange limit for Cu(II)/nitroxyl coupling, the observed *g*-value for a complex containing Cu(II) and *n* ligand radical centres is given by Eq. (1) [2].

$$< g >_{obs} = (n < g >_{L^1} + < g >_{Cu})/(n+1) \quad (1)$$

Since $[Cu(py)_4]^{2+}$ shows $< g > = 2.13$ [21,22,25] and $< g > = 2.006$ for L^1, this gives calculated $< g >_{obs}$ of 2.03, in good agreement with observation. The broad unresolved signals observed here imply that the Cu/L^1 superexchange constant $|J| \geq (< g >_{Cu} - < g >_{L^1})$. From the *Q*-band measurements, we can therefore estimate that $|J| \geq 0.07$ cm^{-1} for **2**. This is at the top of the range previously reported for Cu(II) complexes of TEMPO-substituted pyridines [26].

Because the α- and β-forms of **2** could not be separated manually, variable temperature magnetic susceptibility measurements were performed on a dried powder sample derived from a mixture of both polymorphs. This is reasonable, since the molecular packing in the two structures suggests that they should exhibit similar ferromagnetic and antiferromagnetic contributions to intermolecular superexchange [24]. The observed X_MT for **2** is constant at 1.9 emu mol^{-1} in the range 340–30 K, which agrees well with the theoretical spin-only value for five non-interacting $S = 1/2$ paramagnets of 1.88 emu mol^{-1}. At lower temperatures X_MT decreases, indicating the presence of weak antiferromagnetism within the sample. The magnetic data for **2** were fit to the Curie–Weiss law for five non-interacting $S = 1/2$ paramagnets, which gave a good fit for all data with $g = 2.02$ and $\theta = -0.8$ K. An equally good fit was also obtained using an equation derived by the Kambe vector coupling method [27] according to the scheme of Gatteschi and co-workers [28], using the Hamiltonian in Eq. (2), where *J* describes coupling between the Cu(II) ion (S_1) and nitroxyl spins (S_2–S_5) and J' describes superexchange between adjacent nitroxyl centres (Fig. 5). Fixing $g\{L^1\}$ to 2.00, this model gave $g\{Cu\} = 2.09$ and $J = -0.6$ cm^{-1}; $|J'|$ refined to < 0.1 during the calculation, and so was fixed at 0.

$$H = -2J(S_1S_2 + S_1S_3 + S_1S_4 + S_1S_5) - 2J'(S_2S_3 + S_2S_5 + S_3S_4 + S_4S_5) \quad (2)$$

The excellent agreement obtained from the latter model suggests that intramolecular superexchange may be the major contributor to the magnetic behaviour of **2**. In addition, precedent suggests that antiferromagnetic coupling between the Cu(II) and L^1 spins in **2** is to be expected [28]. However, the value of *J* derived from this analysis is too small to be reliable, and could in fact derive from a combination of intra- and intermolecular couplings. In any case, it is clear from the shape of the X_MT versus T curve (Fig. 5) that there are no detectable ferromagnetic interactions in **2** within the temperature range examined (340–1.8 K). The absence of detectable intermolecular ferromagnetism in solid **2** is surprising given the predominance of N–O…{β-H}–C inter-nitroxyl contacts in the crystal lattices of this compound, and probably reflects loss of crystallinity in the dried material.

In an attempt to confirm the origin of the antiferromagnetism in **2**, variable temperature susceptibility data were also collected for **3**, which contains an identical square planar array of L^1 spins about a diamagnetic ion, as a dried powder. Complex **3** exhibits a high temperature plateau of 1.5 emu mol^{-1} between 340 and 80 K, again in excellent agreement with the theoretical value for four non-interacting spins of 1.50 emu mol^{-1}. Below 80 K, X_MT decreases substantially, at a rate clearly implying the presence of stronger antiferromagnetic interactions compared to **2**. The data for **3** were poorly reproduced by the Curie–Weiss law, which gave $g = 2.03$ and $\theta = -8.3$ K (Fig. 5). No fit to a model describing intramolecular superexchange was attempted, because of the unlikelihood of detectable couplings arising between spins in **3**, which are separated by 18 covalent bonds. The poor Curie–Weiss fit for **3** is suggestive of an efficient intermolecular antiferromagnetic superexchange pathway in this compound, which is retained upon desolvation of the crystal lattice. However, in the absence of a crystal structure for **3**, which might be expected to show a similar distribution of intermolecular N–O…H–C contacts as in the two polymorphs of **2**, it is impossible to suggest what this might be.

Acknowledgements

The authors thank Drs Eric McInnes and Frank Mabbs of the EPSRC CW EPR Service at the University of Manchester for the EPR spectra. The Royal Society (University Research Fellowship to M.A.H.), the Basque government (L.M.R.-M.), the EPSRC (E.K.B. and I.J.S.), the University of Cambridge and St. Catharine's College are acknowledged for financial support.

References

[1] S.S. Eaton, G.R. Eaton, Coord. Chem. Rev. 26 (1978) 207.
[2] S.S. Eaton, G.R. Eaton, Coord. Chem. Rev. 83 (1988) 29.
[3] M.F. Ottaviani, N.D. Ghatlia, S.H. Bossmann, J.K. Barton, H. Dürr, N.J. Turro, J. Am. Chem. Soc. 114 (1992) 8946.
[4] S.U. Dunham, S.J. Lippard, J. Am. Chem. Soc. 117 (1995) 10702.
[5] M.F. Ottaviani, N.D. Ghatlia, N.J. Turro, J. Phys. Chem. 96 (1992) 6075.
[6] M.F. Ottaviani, C. Turro, N.J. Turro, S.H. Bossmann, D.A. Tomalia, J. Phys. Chem. 100 (1996) 13667.
[7] G.K. Anderson, M. Lin, Inorg. Synth. 28 (1990) 60.
[8] G.M. Sheldrick, SHELXTL Plus, An Integrated System for Solving, Refining and Displaying Crystal Structures from Diffraction Data, PC version, Siemens Analytical Instruments Inc., Madison WI, 1990.
[9] G.M. Sheldrick, SHELXL 93, Program for Crystal Structure Refinement, University of Göttingen, 1993.
[10] C.J. O'Connor, Prog. Inorg. Chem. 29 (1982) 203.
[11] SIGMAPLOT, Program for Tabulating, Modelling and Displaying Data (v. 5.0.1), Jandel Scientific, Erkrath, Germany, 1996.
[12] (a) R.A.W. Johnstone, M.E. Rose, Tetrahedron 35 (1979) 2169. (b) D.R. Benedict, T.A. Bianchi, L.A. Cate, Synthesis (1979) 428.
[13] (a) G.R. Newkome, F. Cardullo, E.C. Constable, C.N. Moorefield, A.M.W. Cargill Thompson, J. Chem. Soc. Chem. Commun. (1993) 925. (b) E.C. Constable, A.M.W. Cargill Thompson, P. Harveson, L. Macko, M. Zehnder, Chem. Eur. J. 1 (1995) 360. (c) D. Armspach, M. Cattalini, E.C. Constable, C.E. Housecroft, D. Phillips, Chem. Commun. (1996) 1823. (d) G.R. Newkome, E. He, J. Mater. Chem. 7 (1997) 1237.
[14] M.A. Halcrow, E.K. Brechin, E.J.L. McInnes, F.E. Mabbs, J.E. Davies, J. Chem. Soc. Dalton Trans., in press.
[15] J.-P. Wibaut, W.J. Holmes-Kamminga, Bull. Soc. Chim. Fr. (1958) 424.
[16] (a) A.R. Forster, J.M. Hay, R.H. Thomson, Organic Chemistry of Stable Free Radicals, chapter 5, Academic Press, London, 1968, pp. 180–246. (b) E.G. Rozantsev, V.D. Sholle, Synthesis (1971) 190. (c) J.F.W. Keana, Chem. Rev. 78 (1978) 37.
[17] (a) R. Briere, H. Lemaire, H. Rassat, P. Rey, A. Rousseau, Bull. Soc. Chim. Fr. (1967) 4479. (b) R. Briere, H. Lemaire, H. Rassat, J.-J. Dunand, Bull. Soc. Chim. Fr. (1970) 4220.
[18] P. Tomasik, Z. Ratajewicz, in: G.R. Newkome, L. Strekowski (Eds.), The Chemistry of Heterocyclic Compounds, vol. 14, part 6 (Pyridine–Metal Complexes), Wiley, Chichester, 1985, pp. 186–413 and 1324–1535.
[19] A.B.P. Lever, Inorganic Electronic Spectroscopy, 2nd ed., Elsevier, Amsterdam, 1984, pp. 507–544.
[20] (a) H.P. Fritz, B.M. Golla, H.J. Keller, K.E. Schwarzhans, Z. Naturforsch.Teil B 22 (1967) 216. (b) R.W. Kluiber, W.DeW. Horrocks Jr., Inorg. Chem. 6 (1967) 166. (c) D. Forster, Inorg. Chim. Acta 5 (1971) 465.
[21] C.E. Konig, G. Challa, F.B. Hulsbergen, J. Reedijk, J. Mol. Catal. 34 (1986) 355.
[22] J. Pradilla S., H.W. Chen, F.W. Koknat, J.P. Fackler Jr., Inorg. Chem. 18 (1979) 3519.
[23] (a) J.A. Pretorius, J.C.A. Boeyens, J. Inorg. Nucl. Chem. 40 (1978) 1745. (b) J.S. Haynes, S.J. Rettig, J.R. Sams, J. Trotter, R.C. Thompson, Inorg. Chem. 27 (1988) 1237. (c) M. McCann, E. Murphy, C. Cardin, M. Convery, Polyhedron 11 (1992) 3101. (d) M.J. Jedrzejas, R.L.R. Towns, R.J. Baker, S.A. Duraj, A.F. Hepp, Acta Crystallogr. C 49 (1993) 538. (e) Y. Agnus, M. Labarelle, R. Louis, B. Metz, Acta Crystallogr. C 50 (1994) 536. (f) P. Halasyamani, M.J. Willis, C.L. Stern, P.M. Lundquist, G.K. Wong, K.R. Poeppelmeier, Inorg. Chem. 35 (1996) 1367.
[24] T. Nogami, T. Ishida, M. Yasui, F. Iwasaki, N. Takeda, M. Ishikawa, T. Kawagami, K. Yamaguchi, Bull. Chem. Soc. Jpn. 69 (1996) 1841.
[25] (a) D.H. Brown, R.H. Nuttall, J. McAvoy, D.W.A. Sharp, J. Chem. Soc. A (1966) 892. (b) P.J. Barker, S.R. Stobart, Inorg. Chim. Acta 45 (1980) L197.
[26] Ref. 2, Table 2, pp. 43–44.
[27] K. Kambe, J. Phys. Soc. Jpn. 5 (1950) 48.
[28] A. Caneschi, F. Ferraro, D. Gatteschi, P. Rey, R. Sessoli, Inorg. Chem. 29 (1990) 4217.